PRIFYSGOL ABERYSTWYTH UNIVERSITY

Aberystwyth University

Thickness-dependent electronic structure modulation of ferromagnetic films on shape memory alloy substrates based on a pure strain effect

Feng, Chun; Hu, Di; Gong, Kui; Jiang, Xumin; Yin, Jianjuan; Cao, Yi; Tang, Xiao-Lei; Yang, Feng; Zhou, Zhongfu; Yu, Guanghua; Evans, David

Published in:
Applied Physics Letters

DOI:
10.1063/1.4967996

Publication date:
2016

Citation for published version (APA):
Feng, C., Hu, D., Gong, K., Jiang, X., Yin, J., Cao, Y., Tang, X-L., Yang, F., Zhou, Z., Yu, G., & Evans, D. (2016). Thickness-dependent electronic structure modulation of ferromagnetic films on shape memory alloy substrates based on a pure strain effect. *Applied Physics Letters*, *109*(21), [212401]. https://doi.org/10.1063/1.4967996

General rights
Copyright and moral rights for the publications made accessible in the Aberystwyth Research Portal (the Institutional Repository) are retained by the authors and/or other copyright owners and it is a condition of accessing publications that users recognise and abide by the legal requirements associated with these rights.

• Users may download and print one copy of any publication from the Aberystwyth Research Portal for the purpose of private study or research.
• You may not further distribute the material or use it for any profit-making activity or commercial gain
• You may freely distribute the URL identifying the publication in the Aberystwyth Research Portal

Take down policy
If you believe that this document breaches copyright please contact us providing details, and we will remove access to the work immediately and investigate your claim.

tel: +44 1970 62 2400
email: is@aber.ac.uk

Download date: 09. Jul. 2020

Thickness-Dependent Electronic Structure Modulation of Ferromagnetic Films on Shape Memory Alloy Substrates based on a Pure Strain Effect

Chun Feng[1]*, Di Hu[2]*, Kui Gong[3], Xumin Jiang[1], Jianjuan Yin[1], Yi Cao[1], Xiao-Lei Tang[1], Feng Yang[4], Zhongfu Zhou[2], Guanghua Yu[1,a)], and D. Andrew Evans[2,b)]

[1] *Department of Materials Physics and Chemistry, University of Science and Technology Beijing, Beijing 100083, People's Republic of China*.

[2]*Department of Physics, Aberystwyth University, Aberystwyth, SY23 3BZ, United Kingdom*.

[3] *Centre for the Physics of Materials and Department of Physics, McGill University, Montreal, Quebec H3A2T8, Canada*.

[4] *State Key Laboratory of Heavy Oil Processing, China University of Petroleum-Beijing, Beijing 102249, China*.

Pure strain-induced electronic structure modulation in ferromagnetic films is critical for developing reliable strain-assisted spintronic devices with low power consumption. For the conventional electricity-controlled strain engineering, it is difficult to reveal the pure strain effect on electronic structure tunability due to the inseparability of pure strain effect and surface charge effect. Here, a non-electrically controlled NiTi shape memory alloy was utilized as strain output substrate to induce a pure strain on attached Fe films through a thermally controlled shape memory effect. The pure strain induced electronic structure evolution was revealed by in-situ X-ray photoelectron spectroscopy and correlated with first-principle calculations and magnetic anisotropy measurements. A compressive strain enhances shielding effect for core electrons and significantly tunes their binding energy. Meanwhile, the strain modifies the partial density of states of outer d orbits, which may affect spin-orbit coupling strength and related magnetic anisotropy. This work helps for clarifying the physical nature of the pure strain effect and developing the pure-strain-assisted spintronic devices.

* C. Feng and D. Hu contributed equally to this work.

a) Author to whom correspondence should be addressed. Electronic mail: ghyu@mater.ustb.edu.cn (G.H. Yu)

b) Author to whom correspondence should be addressed. Electronic mail: dne@aber.ac.uk (A. Evans)

In recent years, extensive strain-assisted spintronic materials, which is crucial for developing the spintronic devices with low power consumption, have been achieved based on effective strain engineering[1-22]. Electronic structure of the key ferromagnetic layer in spintronic materials is well modulated by a lattice strain, which causes significant effects on the magnetic/electronic/transport properties of the spintronic materials. Based on the background, pure strain-induced electronic structure modulation in ferromagnetic films becomes the critical issue for developing the reliable strain-assisted spintronic devices. Presently, the most effective strain engineering method to achieve continuous modulation is electrical control of the ferroelectric/ferromagnetic heterostructures [3-8, 10-17]. In this approach, deformation in the ferroelectric substrate, induced by electric field mediated polarization, transfers to the lattice strain in the ferromagnetic overlayer. The electronic structure and related properties of the ferromagnetic film are simultaneously modulated by two effects: strain-mediated magnetoelectric coupling effect (i.e. pure strain effect) and charge-mediated magnetoelectric coupling effect (i.e. surface charge effect), as shown in figure 1a. Here, the surface charge effect is so-called electric-field modulation effect on the magnetism. It is difficult to separate these two effects, although it is possible to tune their relative influence on the modulation by adjusting the ferromagnetic layer thickness [23] or by inserting a non-magnetic layer at the ferroelectric/ferromagnetic interface[7]. Thus, until now, the pure strain-induced electronic structure modulation in ferromagnetic films is difficult to be revealed in order to develop reliable methods for strain engineering in spintronic materials and strain-assisted spintronic devices.

Here, we present a non-electrically controlled method to introduce pure strain in ferromagnetic films using NiTi(Nb) shape memory alloy (SMA) as the substrate material. The substrate deformation derives from a temperature-controlled phase transition from martensite to austenite and this effect has been used to control the lattice strain in the ferromagnetic film as shown in figure 1b. Since the strain modulation in this system originates from the temperature-controlled shape memory effect rather than the electrically-controlled effect, the surface charge effect can be discounted. Moreover, NiTi-based SMAs possess a remarkable strain output as large as 6-8%[24,25] and a short strain generation time ($\sim 10^{-6}$ s), enabling an in-depth study of the pure strain effect on the tunability of electronic structure and related property of the thin film. Fe based composite materials are the critical magnetic layers in many important spintronic devices[26-30] and therefore Fe was chosen as a representative ferromagnetic material in this work. By growing Fe

films on SMA substrates and using the temperature-dependent shape memory effect, the strain in the Fe films can be controlled. The electronic structure modulation in Fe films induced by this pure strain effect has been studied by in-situ X-ray photoelectron spectroscopy (XPS) measurement and first-principle calculations. The results indicate that a compressive strain strengthens the shielding effect from the overlap of outer orbitals, thus modifying the binding energy of core electrons. Additionally, the lattice strain varies the electronic density of states (DOS) distribution of the outer d orbitals, which results in the tunability of the spin-orbit coupling strength and consequent modulation of the magnetic anisotropy of the films.

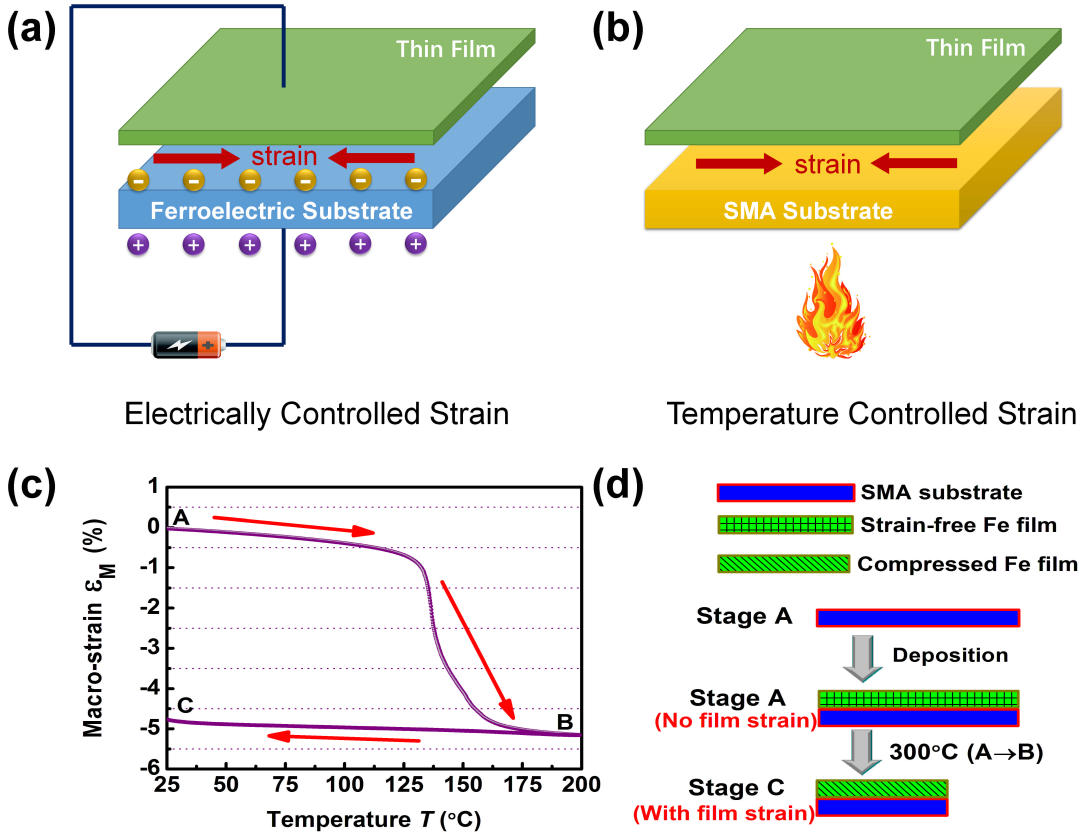

Figure 1 (a) Electrically controlled strain effect from a ferroelectric substrate, where both the strain effect and the surface charge effect coexist. (b) Temperature controlled strain effect from a SMA substrate, where only the strain effect exists. (c) Thermal expansion curve of the pre-stretched SMA substrate to show the thermal history dependence of strains. (d) Schematic diagram of the film deposition and the strain control: an Fe film was deposited on the pre-stretched substrate at room temperature (stage A). Then, the sample was heated to 300℃ to induce a shrinkage deformation in the substrate (A→B) and leading to a nonvolatile lattice strain in the film at room temperature (stage C).

Preparation process: The film deposition and strain control is shown in Figs. 1c-1d. The NiTi(Nb) SMA substrate of composition $Ni_{45}Ti_{45}Nb_{10}$ and thickness 0.5mm was pre-stretched with a 10%

tensile deformation to induced reorientation of the martensite phase. The thermal expansion curve of the substrate, which represents the thermal history dependence of strain, is shown in Fig. 1c. The substrate was polished and then transferred into a ultra-high vacuum chamber for Fe film growth. The pre-stretching process set the initial state A of the substrate in Fig. 1c. A series of Fe films with thickness *t* of 1.5nm, 3.0nm, 5.2nm, 6.5nm, and 8.5nm were deposited on the substrate using a custom-made Knudsen evaporation source in a growth / analysis chamber with a base pressure lower than 10^{-10} mbar. It is inferred from the real-time Ti 2p photoelectron spectra during growth (Fig. S1 in the supplementary material) that the Fe overlayer grows in a Frank-van der Merwe layer-by-layer mode, providing a uniform, strain-free Fe film on the SMA substrate in the as-deposited state. Then, a gradual increase of temperature up to 300℃ induced an inverse martensitic phase transition and shrinkage deformation in the substrate (state A→B) and consequently transferred a nonvolatile, compressive strain onto the attached Fe film even at room temperature (state C). The maximum macro-strain in the substrate was around -5%. The heating rate was controlled around 7-8 ℃/min.

Characterization process: The strain-induced electronic structure variation of inner orbits in the Fe films was studied by in-situ X-ray Photoelectron Spectroscopy (XPS) measurements. A Mg K_α source was used as the incident radiation source, providing x-rays of energy 1253.6 eV. The electron energy analyzer was operated at constant pass energy of 20 eV and calibrated against metal standards. The detection precision of binding energy is controlled as 0.03 eV. Meanwhile, Core level snapshot spectra were collected in real-time electron emission spectroscopy (REES) to monitor the electronic structure evolution in the Fe film during the phase transition process of the substrate. After the XPS measurements, a 5 nm protecting Ta layer was deposited on the Fe layers for subsequent magnetic property measurements. The hysteresis loops were measured by using a physical property measurement system (PPMS) with in-plane (along the strain) or out-of-plane fields up to 20 kOe. First-principle calculations using density functional theory were carried out to simulate the strain-induced tunability effects on DOS distribution of the outer d electrons. The calculation was based on the projector augmented-wave (PAW) from the Vienna ab initio simulation packages (VASP)[31,32] and the Perdew-Burke-Ernzerhof (PBE) exchange-correlation functionals[33]. It includes 2 Fe atoms in BCC unit cell with the lattice constants a = b = c = 2.86 Å. A fine K-mesh at 16 × 16 × 16 and energy cutoff at 500 eV were used to ensure numerical accuracy.

(A) Strain-induced modulation effect on the electronic structure of inner orbits

The strain effect on the electronic structure of the inner Fe 2p core level state was first investigated using in-situ XPS measurements.

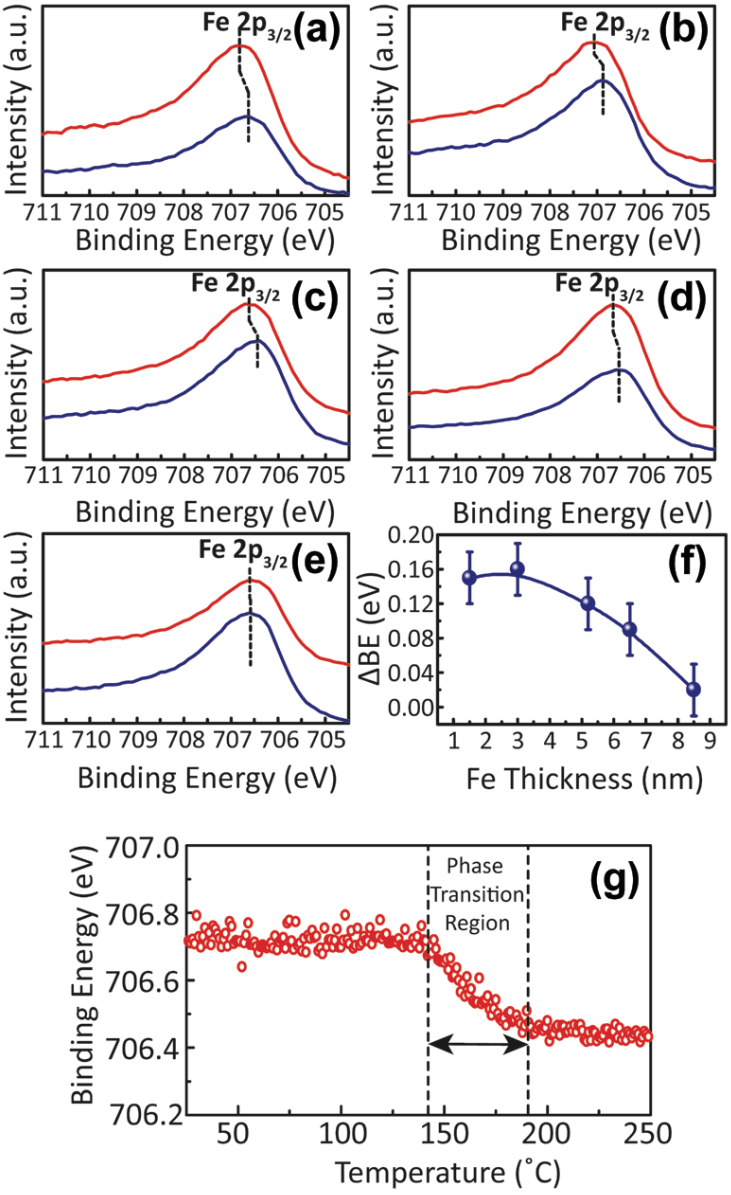

Figure 2 (a-e) High resolution XPS spectra of the Fe2p electrons in the NiTi(Nb)/Fe samples with different film thickness *t*, (a) *t*=1.5 nm; (b) *t*=3.0 nm; (c) *t*=5.2 nm; (d) *t*=6.5 nm; (e) *t*=8.5 nm. The pre-annealing, strain-free state is shown in red and the strain-mediated state obtained by annealing at 300℃ is shown in blue. All the measurements were conducted when samples cooled down to room temperature. (f) The dependence of binding energy variation of $Fe2p_{3/2}$ electrons (ΔBE) with *t*. (g) Variation of $Fe2p_{3/2}$ binding energy with temperature, obtained from real-time XPS spectra of the NiTi(Nb)/Fe (1.5 nm) sample. The phase transition temperature region lies at 130-170℃.

Figure 2 shows the thickness-dependent XPS spectra of Fe 2p electrons in as-deposited films (strain-free state) and 300 ℃ thermal-treated films (compressive strain state). The substrate finishes the phase transition and transfers the compressive strain on the film after the thermal treatment, which can be confirmed by the X-ray diffraction patterns in figure S2 of the supplementary material. As shown in figures 2a-2e, Fe atoms in both the strain-free and the strain-mediated samples are in the elemental state, implying no obvious oxidation or alloying before or after the thermal treatment. However, the Fe $2p_{3/2}$ peak shifts towards lower binding energy on applying the strain to the films, indicating that the compressive strain affects the electronic structure on the inner orbits of the Fe film significantly. For a crystalline material, the outer orbital electrons usually have a shielding effect on inner orbital electrons, which will reduce the effective nuclear charge. When the Fe lattice is compressed, the overlap of the outer electrons between two neighbor Fe atoms will be increased with decreasing interatomic distance, leading to an enhanced shielding and a lower nuclear charge. This will reduce the binding energy of inner electrons, resulting in the XPS peak shift towards lower binding energy.

The binding energy difference of the $Fe2p_{3/2}$ electron between the as-deposited film and the annealed film ($\Delta BE = BE_{As\text{-}deposited} - BE_{Annealed}$) is however dependent on the Fe thickness *t*, as shown in figure 2f. ΔBE is greatest (～0.16 eV) for the thinnest Fe films and is largely unchanged for t ≤ 3.2 nm; it then shows a sharp decrease starting from 3.2 nm. The peak shift almost disappears when *t* reaches 8.5 nm (Fig. 2e). To explain this result, we assume that the strain is non-uniform along the film thickness direction. The strain is a maximum at the NiTi(Nb)/Fe interface and reduces towards the film surface, implying that the strain has an effective interaction depth in the Fe film. For the very thin films with *t* ranging between 1-3 nm, the strain reduction is small. The strain effect on electronic structure therefore extends throughout the film thickness, leading to a large ΔBE value. When the Fe film is thicker than 3 nm, the strain effect starts to reduce exponentially with *t*, resulting in the rapid decrease of ΔBE. For the 8.5 nm film, the strain effect is almost undetectable within the XPS probing depth, $d = 3\lambda$～3.1 nm for normal emission [34]. The maximum detectable position is therefore around 5.4 nm above the NiTi(Nb)/Fe interface in the 8.5 nm Fe film. This value defines the effective interaction depth of the strain effect to be around 5-6 nm for a substrate deformation of 5%. This can be confirmed by the depth-dependent binding energy evolution from the angle-resolved XPS analysis on the strain-treated 5.2 nm Fe film (figure S3 of the supplementary material).

Besides, the thickness-dependent or strain-dependent binding energy variation is well consistent with our computational result (figure S4 of the supplementary material).

In order to further study the strain effect, we monitored the temperature dependence of the electronic structure evolution in the 1.5 nm Fe film using real-time XPS, focusing on the transition induced by the strain change in the substrate. The variation of the binding energy of $Fe2p_{3/2}$ electrons with the temperature is summarized in figure 2g. At temperatures below 130 ℃, the binding energy values fluctuate around 706.7 eV before the onset of the phase transition in the substrate at 130 - 170 ℃. In this region, the substrate shrinks gradually and transfers the changing strain into the Fe film, leading to a pure strain effect on the electronic structure. The phase transition is complete at 170 ℃, with the binding energy stabilized at around 706.5 eV. The XPS results thus confirm that the strain induces significant modulation effect on the electronic structure of inner orbits in the Fe films, leading to an apparent decrease in the binding energy within the effective interaction depth around 5-6 nm. The effective interaction depth under the pure strain effect by SMA substrates is comparable to that under both strain effect and surface charge effect by the conventional ferroelectric substrates.

(B) Strain-induced tunability effect on the electronic structure of outer orbits in Fe films

To reveal the strain effect on the electronic structure of outer orbits in the Fe films, first-principle calculations were performed to simulate the strain-induced evolution of density of states (DOS) distribution.

Figure 3a shows the strain-free bcc-Fe unit cell with lattice constants **a** = **b** = **c** = 2.86 Å. In order to study the strain effect systematically, three lattice compression ratio (ε_L), 0%, -1%, -3%, along [010] or [100] direction were selected. The total DOS in a Fe lattice with ε_L is shown in figure 3b. As the amount of strain increases, the spin distribution of spin-up electrons (↑) moves toward the Fermi level slightly, while the spin-down electrons (↓) moves oppositely. This indicates that the occupied states of spin-up electrons (spin-down electrons) decreases (increases) little when the lattice strain increases, causing a small decrease of the magnetic moment of the Fe crystal (as shown in figure S5 of the supplementary material).

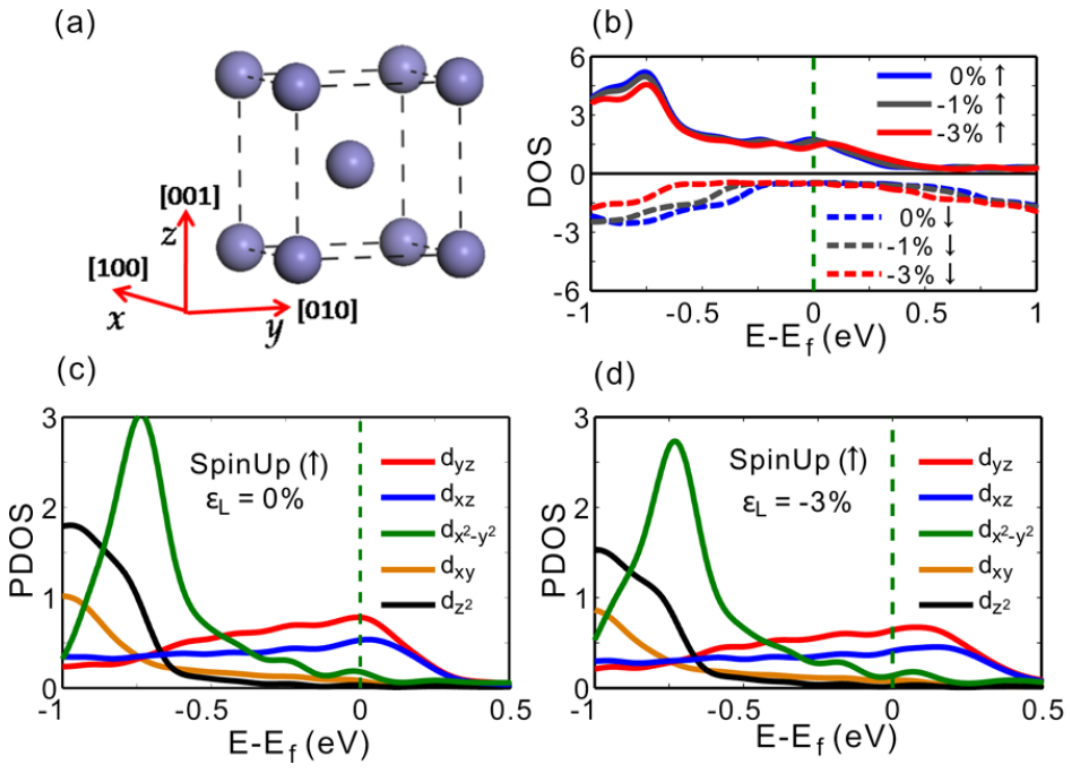

Figure 3 Strain effects on the DOS distribution of the Fe films: (a) ideal strain-free Fe unit cell with **a** = **b** = **c** = 2.86 Å. (b) Total DOS evolution of spin-up (↑) and spin-down (↓) electrons when the unit cell is compressed by 0%, -1%, -3% along the [010] or [100] direction. The dashed line represents the Fermi level. (c) (d) PDOS of different orbitals with a lattice strain (ε_L) of 0% and -3%, respectively.

The partial density of states (PDOS) for different orbitals were also calculated for ε_L = 0% (figure 3c) and ε_L = -3% (figure 3d). For simplicity, only the PDOS of d orbitals are shown because they dominate the states near the Fermi level. For the strain-free bcc Fe crystal, the nearest neighbor Fe atoms are along [111] direction, therefore the d_{xz} or d_{yz} orbitals will have the largest overlap, which leads to the maximum DOS at Fermi level (indicated by the blue and red lines in figure 3c). However, when the Fe lattice is compressed along x or y axis, the $d_{x^2-y^2}$ orbitals increase the overlap, which leads to the dominant bandwidth broadening and largest PDOS intensity decrease on $d_{x^2-y^2}$ orbitals in figure 3d. The dependence of bandwidth broadening on the spin-orbit coupling (SOC) is described by the Thomas SOC strength (equation 1).

$$H_{SO} \equiv \frac{\mu_B}{\hbar m_e e c^2} \frac{1}{r} \frac{dV(r)}{dr} \boldsymbol{L} \cdot \boldsymbol{S} \qquad (1)$$

Where c is the speed of light, m_e is the mass of electron, e is the electron unit charge, V(r) is the electrostatic potential at certain distance r, ***L*** *and* ***S*** are the orbital angular momentum and the spin angular momentum respectively. In the absence of strain, the nearest neighbor Fe atoms have the

largest d orbital overlap along the [111] direction, which leads to the smallest ***L*** and SOC strength according to equation 1. As a consequence, the strain-free Fe crystal will have the smallest SOC energy splitting and hardest magnetization axis in [111] direction, while the easy magnetization axis is along the [001] direction. When a compressive strain is applied on the x-y plane of the Fe unit cell, the d orbital overlap increases, resulting in the reduction of d orbital localization and the decrease of orbital degeneracy. Thus, ***L*** of the d orbital lowers with the strain due to the quenching of d orbital moment [35], leading to a decrease in the SOC strength according to equation 1**.** Since the maximum overlap occurs on $d_{x^2-y^2}$ orbitals in the x-y plane, ***L*** of the $d_{x^2-y^2}$ orbit, that is perpendicular to the x-y plane (i.e. along [001] direction), shows the largest reduction. Therefore, the compressive strain on the (001) plane will tilt the easy magnetization axis of the Fe film away from the [001] orientation, which results in the decrease of the perpendicular magnetic anisotropy of the films. This conclusion can be verified by experimental measurement of the magnetic anisotropy evolution. The thickness-dependent hysteresis loops of the strain-free and strain-treated Fe films are presented in figure 4.

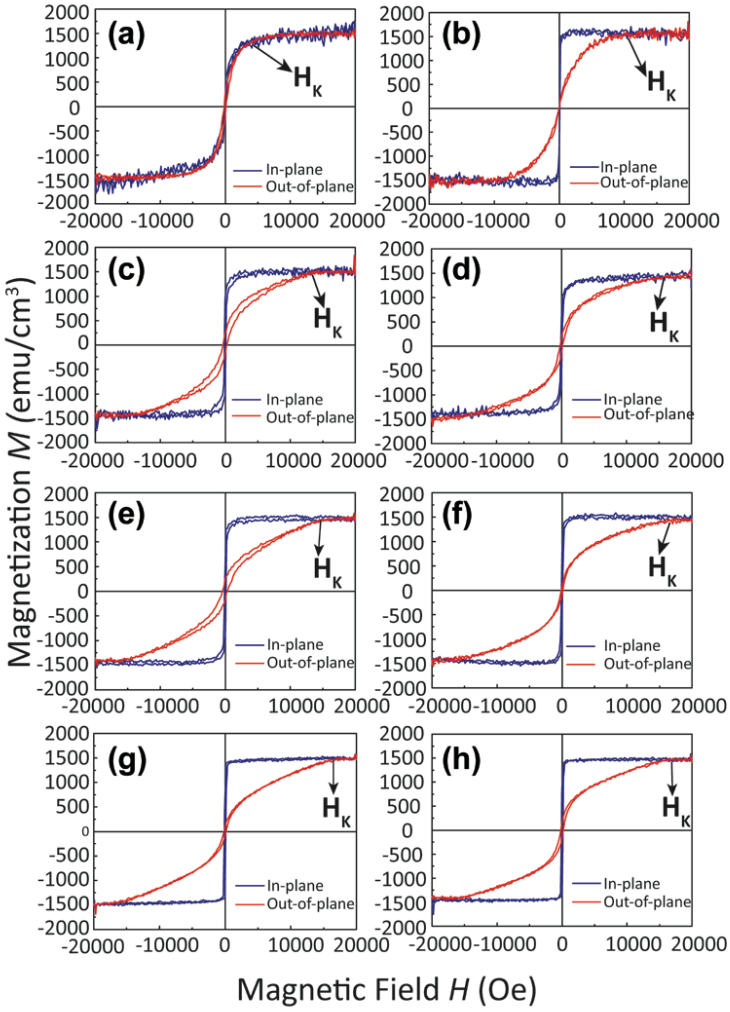

Figure 4 In-plane hysteresis loops (blue curves) and out-of-plane hysteresis loops (red curves) for NiTi(Nb)/Fe (thickness *t*) samples before and after thermal treatments: (a),(b) *t* = 1.5 nm; (c),(d) *t* = 3.0 nm; (e),(f) *t* = 5.2 nm; (g),(h) *t* = 8.5 nm. (a), (c), (e), (g) are for the as-deposited films (strain-free state), and (b), (d), (f), (h) are for the annealed films (strain-treated state).

The intersection of the in-plane loop (blue curve) and out-of-plane loop (red curve), which is marked by an arrow, represents the anisotropy field (H_k) of the film. The effective magnetic anisotropy (K_{eff}) can be calculated by equation 2.

$$K_{eff} = M_S \times H_K / 2, \quad (2)$$

Where M_S is the saturation magnetization of the film. A positive K_{eff} indicates a perpendicular magnetic anisotropy of the film. Figure 5 compares the K_{eff} values of the strain-free and strain-treated Fe films for different Fe thickness. All samples possess negative K_{eff} values, implying an in-plane magnetic anisotropy for each film. The H_k values of most films in figure 4 increase after applying the compressive strain, representing the strain-induced harder magnetization of the films

along the out-of-plane [001] direction. Moreover, K_{eff} values of the strain-treated films are lower than those of the strain-free films with the same thickness, indicating that the compressive strain has an effect of tilting the easy magnetization axis of the film away from the [001] orientation. The result is consistent with the theoretical prediction of the first principle calculations. However, the strain-induced K_{eff} modulation effect is more apparent in the thinner films than in the thicker films, which proves that the strain effect is tunable with an effective interaction depth around 5-6 nm.

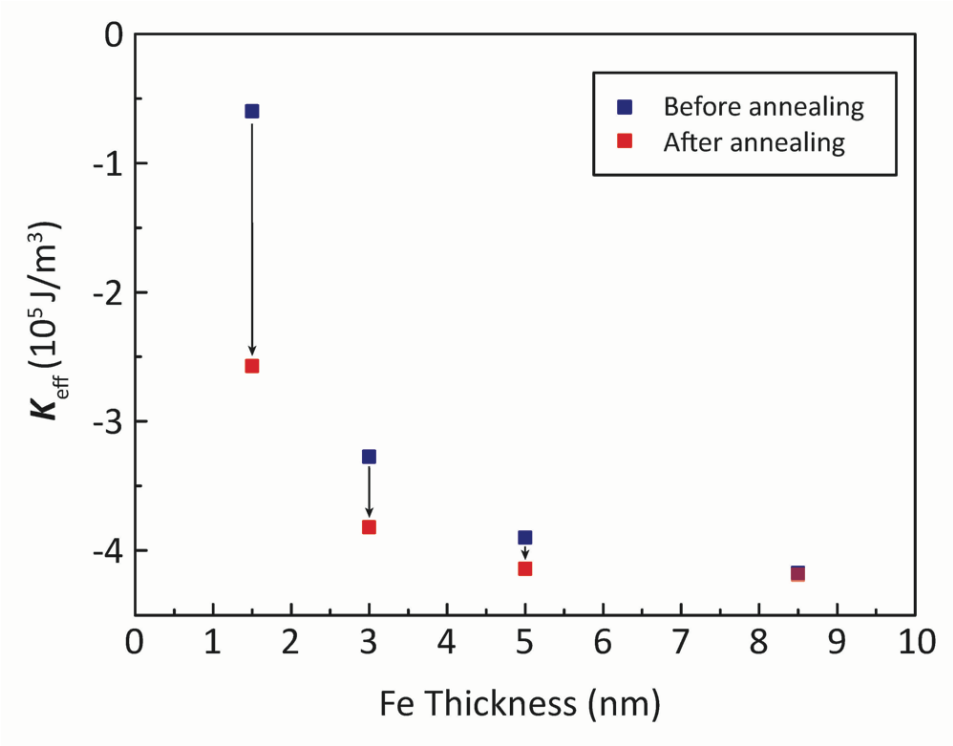

Figure 5 Variation of effective magnetic anisotropy (K_{eff}) of the strain-free and strain-treated Fe films with the film thickness. Blue points and red points represent the as-deposited and annealed samples, respectively.

In summary, pure strain modulation effects on the electronic structure and magnetic anisotropy of ferromagnetic films have been demonstrated by using the non-electrically controlled SMA substrates. The compressive strain in the film modifies the electronic structure of the inner orbitals by enhancing the shielding effect from the outer electrons, resulting in the decrease of binding energy of Fe2p core electrons. Based on first principle calculations, the compressive strain tunes the DOS distribution of outer d orbitals, leading to the evolution of SOC strength and related magnetic anisotropy. This reveals the mechanism of pure strain-induced electronic structure

tunability and also provides a basis for the development of strain-assisted spintronic devices.

Supplementary Material

See supplementary material for the thin film uniformity and growth mode study (figure S1), the strain induced crystal structure evolution (figure S2) and angle-resolved XPS spectra (figure S3), and the computational results on binding energy variation (figure S4) and magnetic moment evolution (figure S5) with the lattice compression ratio.

This work was supported by the National Science Foundation of China (Grant No. 51271211, 51471028, 51671023, 51371027, 51571017), the Beijing Nova program (Grant No. Z141103001814039), and the National key scientific research projects of China (2015CB921502).

[1] J. Li, Z.W Shan, and E. Ma, MRS Bull. **39**, 108 (2014).

[2] J. Feng, X.F. Qian, C.W. Huang, and J. Li, Nat. Photonics **6**, 866 (2012).

[3] M. Weisheit, S. Fahler, A. Marty, Y. Souche, C. Poinsignon, and D. Givord, Science **315**, 349 (2007).

[4] L.H. Diez, A.B. Mantel, O. Michele, L. Via, P. Warin, A. Marty, L. Ranno, and D. Givord, Appl. Phys. Lett. **102**, 012409 (2013).

[5] T. Seki, M. Kohda, J. Nitta, and K. Takanashi, Appl. Phys. Lett. **98**, 212505 (2011).

[6] S. Zhang, Y.G. Zhao, P.S. Li, J.J. Yang, S. Rizwan, J.X. Zhang, J. Seidel, T.L. Qu, Y.J. Yang, Z.L. Luo, Q. He, T. Zou, Q.P. Chen, J.W. Wang, L.F. Yang, Y. Sun, Y.Z. Wu, X. Xiao, X.F. Jin, J. Huang, C. Gao, and X.F. Han, Ramesh, R. Phys. Rev. Lett. **108**, 137203 (2012).

[7] T.X. Nan; Z.Y. Zhou, M. Liu, X. Yang, Y. Gao, B.A. Assaf, H. Lin, S. Velu, X.J. Wang, H.S. Luo, J. Chen, S. Akhtar, E. Hu, R. Rajiv, K. Krishnan, S. Sreedhar, D. Heiman, B.M. Howe, G.J. Brown, and N.X. Sun, Sci. Rep. **4**, 3688 (2014).

[8] Y.Y. Zhao, J. Wang, H. Kuang, F.X. Hu, Y. Liu, R.R. Wu, X. X. Zhang, J.R. Sun, and B.G. Shen, Sci. Rep. **5**, 9668 (2015).

[9] C. Feng, J.C. Zhao, F. Yang, K. Gong, S.J. Hao, Y. Cao, C. Hu, J.Y. Zhang, Z.Q. Wang, L. Chen, S.R. Li, L. Sun, L.S. Cui, and G.H. Yu, Sci. Rep. **6**, 20199 (2016).

[10] A. Mardana, S. Ducharme, and S. Adenwalla, Nano Lett. **11**, 3862 (2011).

[11] Y.G. Zhou, Z.G. Wang, P. Yang, X.T. Zu, L. Yang, X. Sun, and F. Gao, ACS Nano **6**, 9727 (2012).

[12] L.M. Loong, X.P. Qiu, Z.P. Neo, P. Deorani, Y. Wu, C.S. Bhatia, M. Saeys, and H. Yang, Sci. Rep. **4**, 6505 (2014).

[13] A. Tkach, A. Kehlberger, F. Büttner, G. Jakob, S. Eisebitt, and M. Kläui, Appl. Phys. Lett. **106**, 062404 (2015).

[14] A.M. Sahadevan, R.K. Tiwari, G. Kalon, C.S. Bhatia, M. Saeys, and H. Yang, Appl. Phys. Lett. **101**, 042407 (2012).

[15] X. He, L. Gao, N. Tang, J.X. Duan, F. J. Xu, X.Q. Wang, X.L. Yang, W.K. Ge, and B. Shen, Appl. Phys. Lett. **105**, 083108 (2014).

[16] C.J. Jiang, C. Zhang, C.H. Dong, D.W. Guo, and D.S. Xue, Appl. Phys. Lett. **106**, 122406 (2015).

[17] J.S. Chen, B.C. Lim, Y.F. Ding, and G.M. Chow, J. Magn. Magn. Mater. **303**:309 (2006).

[18] R.S. Jacobsen, K.N. Andersen, P.I. Borel, J.F. Pedersen, L.H. Frandsen, O. Hansen, M. Kristensen,

A.V. Lavrinenko, G. Moulin, H. Ou, C. Peucheret, B. Zsigri, and A. Bjarklev, Nature **441**, 199 (2006).
[19] R.J. Zeches, M.D. Rossell, J.X. Zhang, A.J. Hatt, Q. He, C.-H. Yang, A. Kumar, C.H. Wang, A. Melville, C. Adamo, G. Sheng, Y.-H. Chu, J. F. Ihlefeld, R. Erni, C. Ederer, V. Gopalan, L.Q. Chen, D.G. Schlom, N.A. Spaldin, and L.W. Martin, Science **326**, 977 (2009).
[20] Z.H. Tang, B.M. Wang, H.L. Yang, X.Y. Xu, Y.W. Liu, D.D. Sun, L.X. Xia, Q.F. Zhan, B. Chen, M.H. Tang, Y.C. Zhou, J.L. Wang, and R.-W. Li, Appl. Phys. Lett. **105**, 103504 (2014).
[21] G.H. Dai, Q.F. Zhan, Y.W. Liu, H.L. Yang, X.S. Zhang, B. Chen, and R.-W. Li, Appl. Phys. Lett. **100**, 122407 (2012).
[22] C. Feng, J.C. Zhao, F. Yang, S.J. Hao, K. Gong, D. Hu, Y. Cao, X.M. Jiang, Z.Q. Wang, L. Chen, S.R. Li, L. Sun, L.S. Cui, and G.H. Yu, ACS Appl. Mater. Inter. **8**:7545 (2016).
[23] L. Shu, Z. Li, J. Ma, Y. Gao, Y. Shen, Y.H. Lin, and C.W. Nan, Appl. Phys. Lett. **100**, 022405 (2012).
[24] K. Otsuka, and X. Ren, Prog. Mater. Sci. **50**, 511 (2005).
[25] S.J. Hao, L.S. Cui, D.Q. Jiang, X.D. Han, Y. Ren, J. Jiang, Y.L. Liu, Z.Y. Liu, S.C. Mao, Y. D. Wang, Y. Li, X.B. Ren, X.D. Ding, S. Wang, C. Yu, X.B. Shi, M.S. Du, F. Yang, Y.J. Zheng, Z. Zhang, X.D. Li, D.E. Brown, and J. Li, Science **339**, 1191 (2013).
[26] N. Nagaosa, J. Sinova, S. Onoda, A.H. MacDonald, and N.P. Ong, Rev. Mod. Phys. **82**, 1539 (2010).
[27] X.P. Qiu, K. Narayanapillai, Y. Wu, P. Deorani, D.-H. Yang, W.-S. Noh, J.-H. Park, K.-J. Lee, H.-W. Lee, and H. Yang, Nat. Nanotechno. **10**, 333 (2015).
[28] K.M. Seemann, Y. Mokrousov, A. Aziz, J. Miguel, F. Kronast, , W. Kuch, M.G. Blamire, A.T. Hindmarch, B.J. Hickey, I. Souza, and C.H. Marrows, Phys. Rev. Lett. **104**, 076402 (2010).
[29] X. Fan, J. Wu, Y.P. Chen, M.J. Jerry, H.W. Zhang, and J.Q. Xiao, Nat. Commun. **4**, 1799 (2013).
[30] T. Jungwirth, J. Wunderlich, and K. Olejník, Nat. Mater. **11**, 382 (2012).
[31] G. Kresse, and J. Hafner, Phys. Rev. B **47**, 558 (1993).
[32] P.E. Blochl, Phys.Rev. B **50**, 17953 (1994).
[33] J.P. Perdew, K. Burke, and M. Ernzerhof, Phys. Rev. Lett. **77**, 3865 (1996).
[34] S. Tanuma, C.J. Powell, and D.R. Penn, Surf. Interface Anal. **11**, 577 (1988).
[35] J. Stohr, J. Magn. Magn. Mater. **200**: 470 (1999).